Boletín de la Sociedad Española de Cerámica y Vidrio
Vol 51, 4, 211-216, Julio-Agosto 2012 ISSN 0366-3175. eISSN 2173-0431.
doi: 10.3989/cyv.302012

BOLETIN DE LA SOCIEDAD ESPAÑOLA DE
Cerámica y Vidrio
A R T I C U L O

Ultrasonic characterization of defective porcelain tiles

E. EREN[1], S. KURAMA[*,1], R. JANSSEN[2]

[1] Anadolu University, Faculty of Engineering and Architecture, Department of Materials Science and Engineering, Iki Eylul Campus, 26555, Eskisehir/TURKEY [*]Corresponding author. : skurama@anadolu.edu.tr (S. Kurama)
[2]Advanced Ceramics Group, Technische Universität Hamburg-Harburg 21071 Hamburg/GERMANY

The aim of this work is the optimization of ultrasonic methods in the non-destructive testing of sintered porcelain tiles containing defects. For this reason, a silicon nitride ball, carbon black and PMMA (Polymethylmethacrylate) were imbedded in porcelain tile granules before pressing to make special defects in tiles. After sintering at 1220˚C, the time of flight of the ultrasonic waves and ultrasonic signal amplitudes through the sintered porcelain tiles were measured by a contact ultrasonic transducer operating on pulse-echo mode. This method can allow for defect detection using the A-scan. The results of the test showed that the amplitude of the received peak for a defective part is smaller than for a part which has no defects. Depending on the size, shape and position of the defect, its peak can be detected. Additionally, an immersion pulse-echo C-scan method was also used to differentiate between defects in porcelain tiles. By using this technique, it is possible to determine the place and shape of defects. To support the results of the ultrasonic investigation, a SEM characterization was also made.

Keywords: Porcelain tile, defect, ultrasonic A-scan, ultrasonic C-scan, SEM characterization.

Caracterización ultrasónica de los azulejos defectuosos de la porcelana

El fin principal de este trabajo es la optimización de métodos ultrasónicos en la prueba no destructiva de azulejos sinterizados de porcelana que contienen defectos. Por lo tanto, bolas del nitruro de silicio, negros de carbón y PMMA (polimetilmetacrilato) fueron encajados en gránulos del azulejo de porcelana antes de presionar para hacer defectos especiales en azulejos. Después de sinterizado en 1220˚C, el tiempo de vuelo de las ondas ultrasónicas fue medido a través del azulejo sinterizado de la porcelana. El tiempo del vuelo de ondas ultrasónicas fue medido por un transductor de contacto ultrasónico operando en modo eco-pulso. Este método puede permitir la detección de defectos usando escaneo-A. Los resultados de la prueba demostraron que la amplitud del pico recibido por partes defectuosas es más pequeño que la parte que no tiene defectos. Dependiendo del tamaño, de la forma y de la posición del defecto. Su pico puede ser detectado. Además, un eco-pulse de inmersión de del método pulse-echo escaneo-C también fue utilizado para distinguir defectos en azulejos de porcelana. Usando esta técnica es posible determinar el lugar y la forma de los defectos. Para apoyar resultados de la investigación ultrasónica, una caracterización SEM también fue realizada.

Palabras clave: El azulejo de porcelana, defecto, ultrasónico escaneo-A, ultrasónico escaneo-C, la caracterización SEM.

1. INTRODUCTION

Although historically nondestructive techniques (NDT) have been used almost exclusively for the detection of macroscopic defects in structures after they have been in service for some time, it has become increasingly evident that it is both practical and cost effective to expand the role of nondestructive evaluation to include all aspects of materials production and application. Currently, efforts are being directed at developing and perfecting nondestructive evaluation techniques which are capable of monitoring and controlling the materials production process; the materials stability during transport, storage, and fabrication, and the amount and rate of degradation of the materials during their service life (1).

Due to a discontinuity of detection and material characterization in various engineering fields, ultrasonic testing is a versatile NDT method, applicable to most materials, whether metallic or non-metallic (2, 3). Measurement procedures initially developed for metals have been extended to engineered materials, such as composites, where anisotropy and homogeneity have become important issues (4). The determination of ultrasonic velocities can be used to measure the modulus of elasticity or Young's modulus of materials, monitor the development of thermal shock damage, characterize indirectly fracture toughness, R-curve behavior, hardness depending on heat treatment, volume fraction porosity and density (5-21). Recently, the ultrasonic test has also been used to detect internal flaws in ceramics and other materials (22).

A number of ultrasonic evaluation methods, such as A-, B-, and C-scans can be used to study various types of flaw in ceramic materials. The UT A-scan presents one-dimensional defect information. With the oscilloscope view, the A-scan

signal displays pulse and amplitude against time obtained at a single point on the surface of the test piece which can be used to analyze the type, size and location (chiefly depth) of flaws. The UT-B scan displays a parallel set of UT A-scans with two-dimensional data (i.e., the B-scan presents defect distribution through the material's cross section). The UT C-scan is the most widely-used scanning mode, as it provides a two-dimensional presentation of defect distribution obtained over an area of the test-piece surface (4, 5). This information can be used to map out the position of flaws on a plan view of the test-piece. A C-scan format also records time-of-flight data, which can be converted and displayed by image-processing equipment to provide an indication of flaw depth (23).

The reliability of ceramic materials can be enhanced by an accurate rejection of products that contain critical defects. Three main flaws currently found in ceramic works are cracks, porosity, and inclusions; density and structural variations may also greatly impair component performance in particular situations. Quality control of the sintered material was therefore achieved by means of ultrasonic images allowing defect detection (24). Bhardwaj and et al. investigated defected ceramics. In order to determine the feasibility and detectability of defects in non-contact ultrasonic mode, 1.5 mm diameter side drilled cylindrical holes were made in green and sintered ceramics. From observation of these, it is apparent that when ultrasound encounters a discontinuity in its path of propagation, the amount of energy transmitted is reduced, relative to that from a defect-free region (25). Bhardwaj also investigated defect free and internal cracks containing porous ZrO_2 refractories. The refractories visually looked alike. However, when they were examined ultrasonically, one produced results typical of internal cracks. The amplitude of ultrasonic signals decreased with the presence of cracks (26). Romagnoli and et al. investigated detecting the delamination of green and fired ceramic tiles using ultrasonic pulse velocity measurement. They assumed that an increase in travel time for a given thickness (i.e., decrease in travel velocity) would indicate the presence of delamination, as the sound wave has to travel around the flat pore (27). High-frequency ultrasound NDT is being used to locate micron-range defects, as well as to identify microstructural changes in dense armor ceramics. While time of flight scans have been used to show changes in thickness, acoustic wave velocity, density and acoustic impedance, reflected signal amplitude scanning has recently been employed to analyze attenuation or loss through a test specimen (28). Brennan and et. al. characterized three SiC samples of varying thickness, fabricated different fabrication routes, with these being characterized using pulse-echo ultrasound. C-scan imaging was used to evaluate differences in both time of flight and reflected signal amplitude over the area of each sample. The results of the study emphasize the importance of utilizing both reflected signal amplitude and time of flight C-scan imaging to obtain a full range of ultrasound data for sample comparison (29).

In this study, two ultrasonic methods (A- and C-scans) were used in the detection of different defect types of porcelain tile. Therefore, the defect effect on ultrasonic wave attenuation was characterized. Additionally, the results were supported by SEM analysis.

2. EXPERIMENTAL PROCEDURE

Standard porcelain tile granules were used in the preparation of samples in this study. The samples were prepared by the uniaxial pressing technique in a 50 mm x 100 mm rectangular die by applying 450 kg/cm^2 pressure, and then dried at 110ºC. The Si_3N_4 ball (2.9 mm), C black (5-10 μm particles) and PMMA (0.1-0.3 mm particles) were placed into Tile 1, Tile 2 and Tile 3, respectively. Sintering was carried out in a laboratory kiln (Protherm plf 150/9) at 1220ºC.

An Olympus Panametrics-NDT Model 5800 Computer Controlled Pulser/Receiver was used for measurement of the ultrasonic time of flight (t). The time of flight of the ultrasonic waves (longitudinal waves) was measured using a 1.27cm diameter contact ultrasonic transducer operating on pulse-echo mode. The flight time is determined through the thickness of the tile, which includes the time of the sent ultrasonic signals from the top surface reaching to the bottom of the tile and being reflected back (Fig. 1). The center frequency of the transducer was 5 MHz. In this technique, glycerol was used as a couplant material. The transit time was determined with an accuracy of ± 40 nsec. To measure the number of dB or loss, the amplitudes of the backwall echoes were used according to this equation (30):

$$\text{number of dB} = 10\log_{10}\left|\frac{A_1}{A_0}\right|^2 = 20\log_{10}\left|\frac{A_1}{A_0}\right| \qquad [1]$$

where, A_1 is the amplitude of the defect and A_0 is the amplitude defect-free parts of the inspected tiles. For the C-scan analysis, the Dr. Hillger USPC 3040 DAC Industrie system was used. C-scan imaging was performed on the aforementioned tiles using a 6-12 MHz longitudinal focused immersion transducer. The transducer had a diameter of 0.6 cm and a focal length of 15 cm. Tiles were placed in an immersion tank and the z-position was manually adjusted until the maximum signal was obtained. The top and bottom surface peak reflections were identified on the oscilloscope, and the bottom surface signal was gated so that the variation of the signal could be collected as it traveled through each tile in the x-y scanning frame. Using this technique, ultrasonic amplitude measurements were performed using the pulse-echo C-scan mode. As a result of these measurements, the failure position and attenuation loss for failure and backwall echo images were drawn. While failure echo images are drawn with the failure echo peaks, backwall echo images are drawn with the backwall echo peaks. The relative attenuation loss range changed from 0 dB (greatest amplitude) to - dB values (least relative amplitude). For the failure echo 0 dB shows the areas attenuated by the defects, but for the backwall echo 0 dB

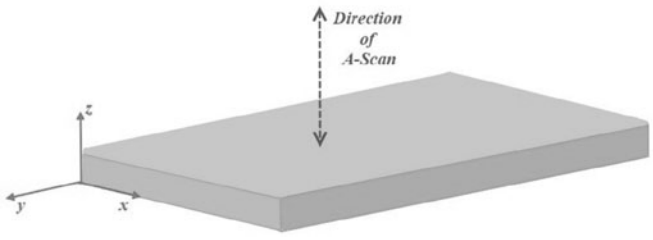

Figure 1. Ultrasonic A-scan measurements through the tile.

shows 'good' or 'dense' regions. Failure positions show the place of the defect through the thickness' of the tiles from the top surfaces of the tiles.

A conventional technique, scanning electron microscopy (SEM), is commonly used to characterize the microstructure of ceramics (31). In our study sintered samples were cut in parts. For the SEM observations, a scanning electron microscope (SEM) (Zeiss Supra TM 50 VP) was used in a secondary electron (SE) imaging mode. By measurement of the scanning electron microscope (SEM), characterization images for the distance between the defect and the surface supported by defect position information were obtained with the ultrasonic A and C-scan.

3. RESULTS AND DISCUSSION

In order to determine the feasibility and detectability of defects using the contact ultrasonic mode, defects were imbedded in sintered ceramics. Fig. 2 (a) shows typical transmitted ultrasonic signal as a function of the defect-free part in the Si_3N_4 ball containing the sintered tile (Tile 1). The time of flight (t) for the defect-free part is 2.8 μs and the amplitude of the backwall echo is 55.2 V. Fig. 2 (b) represents a typical transmitted ultrasonic signal as a function of the defective region in the Si_3N_4 ball containing the sintered tile. The time of flight through the defective part of the tile is the same as the time of flight through the defect-free part. The sound waves travel through the tile (with some attendant loss of energy) and are deflected at interfaces and/or defects. The deflected beam can be displayed and analyzed to assess the presence of flaws or discontinuities (5). The Si_3N_4 ball defect is smaller than the diameter of the transducer and the defect did not alter the time of flight, but the defect decreased the amplitude of the backwall echo to 52.4 V. Therefore, the Si_3N_4 ball defect was calculated as a -0.45 dB loss at the amplitude of the wave in the measurement area of the transducer using Equation 1. This resulted in a low echo which was observed due to the Si_3N_4 ball in Fig. 2 (b). It is difficult to see the Si_3N_4 ball defect in Fig. 3 (a, c) because the ball is spherical and reflects ultrasonic signals with different angles (32). Due to this reflection, the Si_3N_4 ball prevented ultrasonic signals

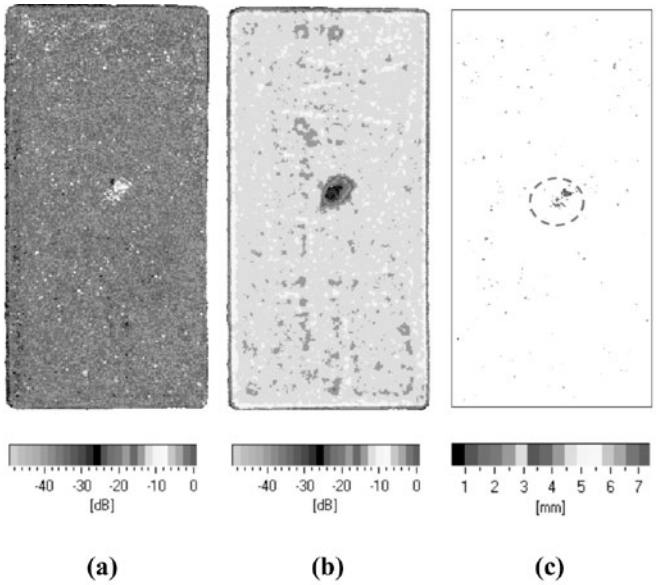

Figure 3. C-scan displays showing the failure echo (a), the backwall echo (b), and the failure position (c) part in the Si3N4 ball containing the sintered tile.

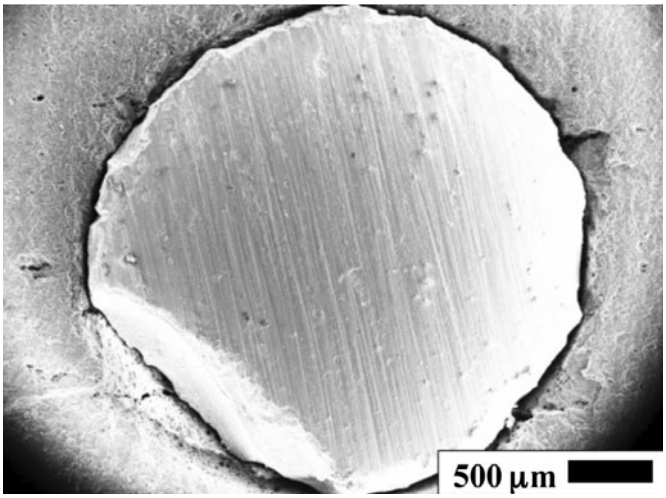

Figure 4. SE image of a Si_3N_4 ball defect.

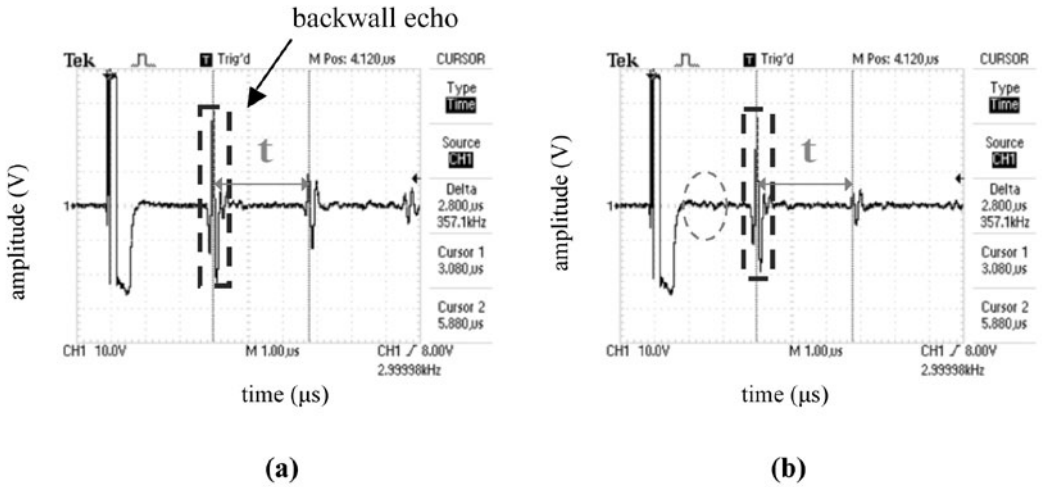

Figure 2. A-scan displays showing the time of flight representing the defect-free (a), and the defective (b) part in the Si_3N_4 ball containing the sintered tile.

passing completely to the backwall, increased attenuation loss (to -30dB), and can be seen in the backwall echo (Fig. 3 (b)). For the failure echo, the ball created attenuation varying from -2 to -28 dB. Due to the low values of these echoes, being very close to 0 dB, it is not easy to determine the defect in the tile. The Si_3N_4 ball stayed spherical during firing (Fig. 4). The distance and depth of the Si_3N_4 ball in Tile 1 are not achieved using the ultrasonic A- and C-scan.

Fig.5 (a) shows a typical transmitted ultrasonic signal as a function of the defect-free part in the C black containing the sintered tile (Tile 2). The time of flight for the defect-free part is 2.72 μs. Fig. 5 (b) represents a typical transmitted ultrasonic signal as a function of the defective region in the C black containing the sintered tile. The time of flight through the defective part of the tile is the same as the time of flight through the defect-free part. The C black defect is smaller than the diameter of the transducer and the defect does not alter the time of flight. In Fig. 5 (b), there is a high echo due to the C black. Due to this high echo, the amplitude of the backwall echo decreased from 41.6 V to 30 V. The signals reflected from the defect are also seen in Fig. 5 (b) and can be used to determine the depth of the defect position. The difference in times of flight between the signal reflected from the defect and the backwall echo is measured as t_1=1.6 μs in Figure 5 (b). Therefore, the defect position is 4.49 mm beyond the bottom plane of the specimen. The thickness of tile is 7.62 mm and the defect is 3.13 mm from the surface of tile.

When decibel calculation is performed with reference to amplitude (41.6 V) and measured amplitude (30 V) using Equation 1, the C black defect created a -2.84 dB loss at the amplitude of the wave in the measurement area of the transducer. The defect can be seen in Fig. 6 (a, b, c). For the failure echo, the C black defect created attenuation varying from 0 to -24 dB. In the C black defect, the echoes close to 0 dB are higher than that of the Si_3N_4 ball defect. Therefore, it is possible to see the defect in tile. The backwall echo image was attenuated to nearly -28 dB in Fig. 9 (b) by the C black defect. The C black was distributed throughout Tile 2 and it appears in only a few parts at 1.8-2.2 mm thickness but the main part appears at 2.7-4 mm thickness. When the defect's distance to the surface is measured with the SEM (Fig. 7), it is 3.08 mm. This value is appropriate with the failure place shown in Fig. 6 (c).

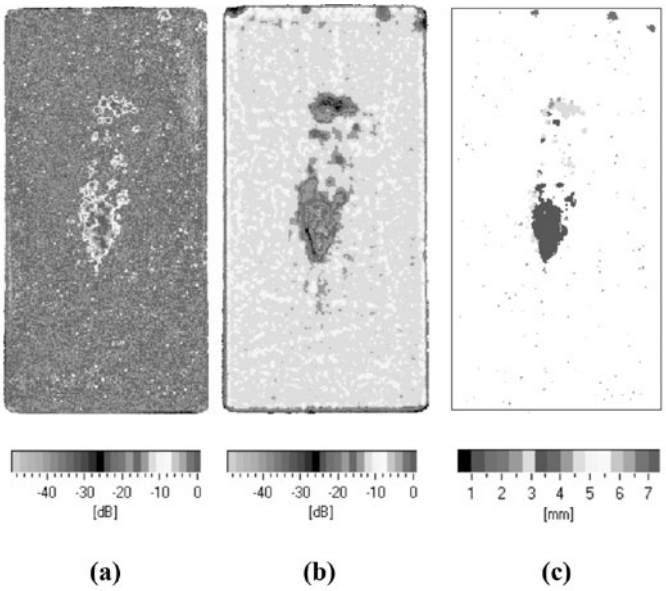

Figure 6. C-scan displays showing the failure echo (a), the backwall echo (b), and the failure position (c) part in the C black containing the sintered tile.

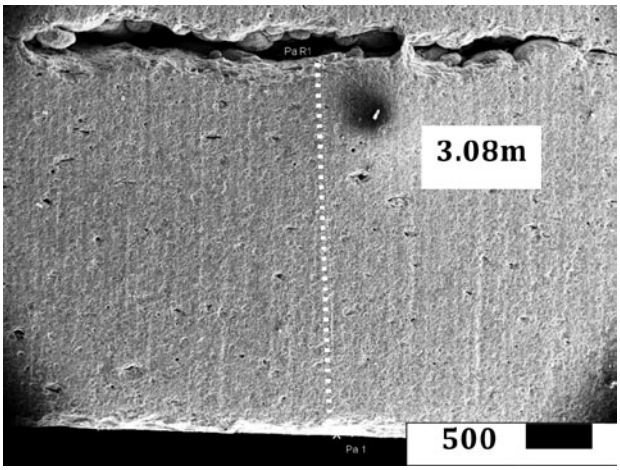

Figure 7. SE image of C black defect.

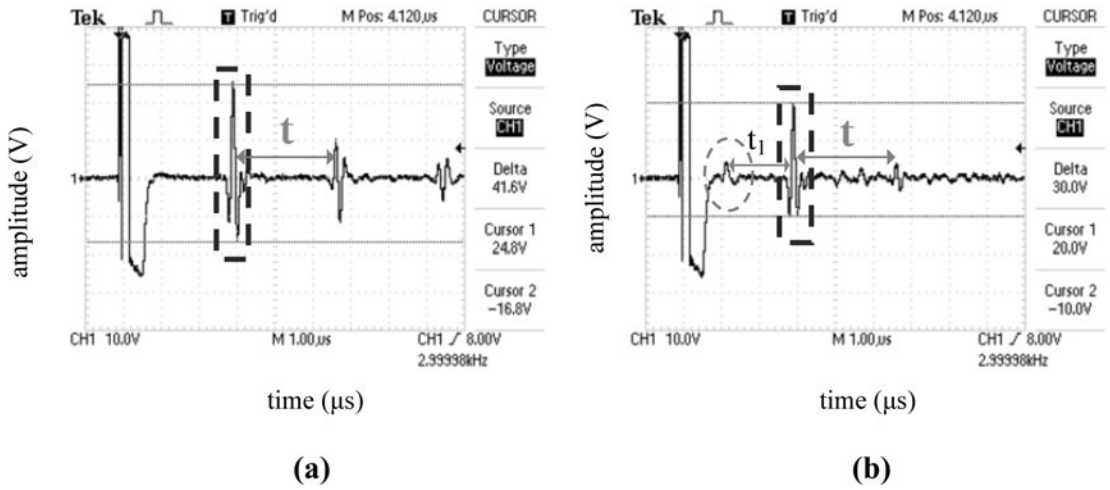

Figure 5. A-scan displays showing the time of flight representing the defect-free (a), and the defective (b) part in the C black containing the sintered tile.

Bol. Soc. Esp. Ceram. Vidr. Vol 51. 4, 211-216, Julio-Agosto 2012. ISSN 0366-3175. eISSN 2173-0431. doi: 10.3989/cyv.302012

Fig.8 (a) shows a typical transmitted ultrasonic signal as a function of the defect-free part in the PMMA containing the sintered tile. The time of flight for the defect-free part is 2.64 μs. Fig. 8 (b) represents a typical transmitted ultrasonic signal as a function of the defective region in the PMMA containing the sintered tile. The time of flight through the defective part of the tile is not measured. When the backwall signal is inspected (square) in Fig. 8 (b), it is smaller than the failure signal (sphere). The signals reflected from the defect are also seen in Fig. 8 (b) and can be used for determining the depth of the defect position. The difference in times of flight between the signal reflected from the defect and the backwall echo is measured as t_1=1.32 μs in Figure 8 (b). The defect is in the middle of the 7.40 mm thick tile. The PMMA defect's size is greater than the diameter of the transducer and the defect prevents the ultrasonic signal's from passing through. So, the amplitude of the backwall echo decreased from 64 V to 4 V.

When decibel calculation is performed with reference to amplitude (64 V) and measured amplitude (4 V) using Equation 1, the PMMA defect created a -24.08 dB loss at the amplitude of the wave. In Fig. 8 (b), there is a high echo due to the PMMA. The defect can be seen in the PMMA containing the sintered tile in Fig. 9 (a, b, c). The PMMA appeared in the middle of Tile 3. The failure echo image attenuated from 0 to -28 dB in Fig. 9 (a) and the highest echoes closing to 0 dB were observed for this defect. The backwall echo image attenuated to nearly -30 dB in Fig. 9 (b) by the PMMA defect. The failure position changes from between 2.6-4.2 mm in Fig. 9 (c). When the defect's distance to the surface is measured with the SEM (Fig. 10), it is 3.07 mm. This value is appropriate with the failure position shown in Fig. 9 (c).

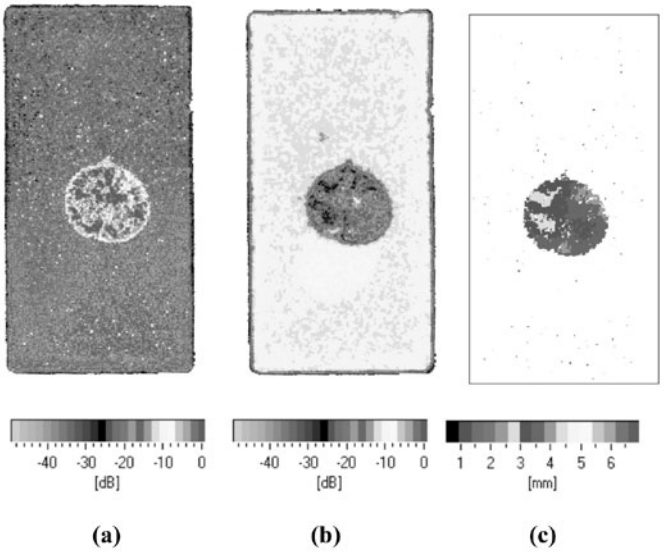

Figure 9. C-scan displays showing the failure echo (a), the backwall echo (b), and the failure position (c) part in the PMMA containing the sintered tile.

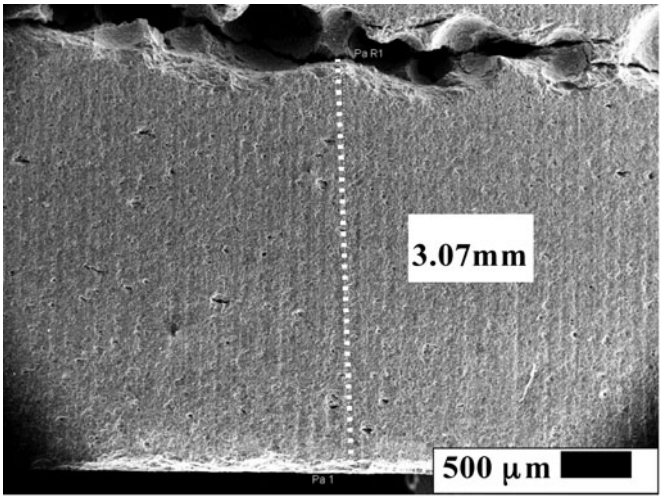

Figure 10. SE image of PMMA defect.

4. CONCLUSION

The detection and characterization of defects were achieved by optimization of the use of ultrasonic techniques for the non-destructive characterization of materials. Using the A-scan, different defects were detected. Shape and size are critical factors for detection. While the Si_3N_4 spherical ball was difficult to detect due to reflections resulting from its spherical

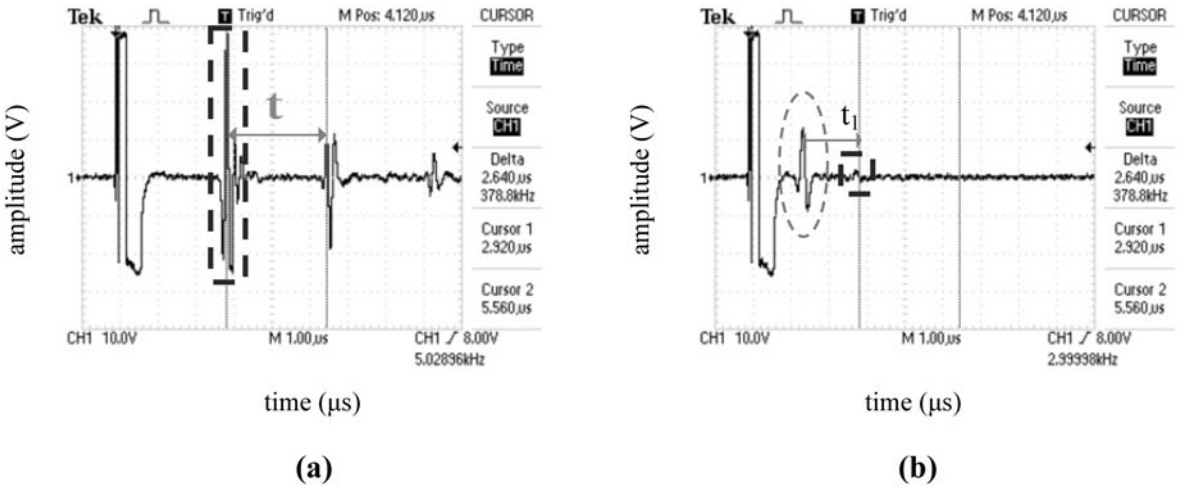

Figure 8. A-scan displays showing the time of flight representing the defect-free (a), and the defective (b) part in the PMMA containing the sintered tile.

shape, the PMMA and carbon black were easily detected using the A-scan. The results of the study demonstrate that shape and size of defects determine dB losses. The PMMA defect is greater than the size of transducer, so the PMMA defect made a dB loss 10 times greater at the amplitude of the wave compared with C black defect and a dB loss 50 times greater at the amplitude of the wave compared with the Si_3N_4 spherical ball defect.

Evaluation and quantification of these defects were obtained using the ultrasonic C-scan. The attenuation loss of ultrasonic waves changes with the defects' deflection and the scattering of the waves. When failure echo images were compared, the highest echoes closing to 0 dB were observed for the PMMA defect, meaning the PMMA made the highest loss at attenuation. All defects were clearly detected via the backwall echo images.

In the failure position results obtained using the C-scan, different colors were assigned to the various time-of-flight ranges to indicate the depth of the defects in the sample. A-scan and SEM results, showing the distance between the surface and the failure for the defect position, are in between failure places measured using the ultrasonic C-scan for the C-black defect and the PMMA defect. Consisting of particles, these defects spread various thicknesses in the tiles. The effect of thickness is clearly seen in the C-scan failure position images. For the Si_3N_4 ball, the defect position is not measured using ultrasonic techniques due to the reflections from the spherical surface.

As a result, defects which are perpendicular to the ultrasonic waves can be easily detected using the ultrasonic A and C-scans.

ACKNOWLEDGEMENTS

The financial support from the Anadolu University Scientific Research Project, project 080210, is gratefully acknowledged. The authors would like to thank Research Assistant Şükrü Görgülü from Anadolu University, Dipl. -Ing. Wilfried Liebig and Prof. Dr. Karl Schulte from the Technische Universität Hamburg-Harburg.

REFERENCES

(1) A. Vary (Ed.), Materials Analysis by Ultrasonics: Materials, Ceramics, Composites, Noyes Data Corporation, Park Ridge, New Jersey, U.S.A., 1-15 (1987)
(2) B. Raj, T. Jayakumar, M. Thavasimuthu, Practical Non-Destructive Testing, 2nd ed., Alpha Science International Ltd., Pangbourne, England, 77 (2002)
(3) R. Franklin, U. B. Halabe, B. Gopalakrishnan, NDT solution, knowledge based assistant for ultrasonic testing methodology of materials, The American Society for Nondestructive Testing (2001) (http://www.asnt.org/publications/materialseval/solution/dec01solution/dec01sol.htm)
(4) Present State of Ultrasonics, http://www.ndt-ed.org (http://www.ndt-ed.org/EducationResources/CommunityCollege/Ultrasonics/Introduction/presentstate.htm)
(5) J. Kim, P. K. Liaw, The nondestructive evaluation of advanced ceramics and ceramic-matrix composites, JOM, 50, 11 (1998)
(6) P. Pialy, N. Tessier-Doyen, D. Njopwouo, J. -P. Bonnet, Effects of densification and mullitization on the evolution of the elastic properties of a clay-based material during firing, J. Eur. Ceram. Soc., 29, 9, 1579-1586 (2009)
(7) D. N. Boccaccini, M. Romagnoli, E. Kamseu, P. Veronesi, C. Leonelli, G. C. Pellacani, Determination of thermal shock resistance in refractory materials by ultrasonic pulse velocity measurement, J. Eur. Ceram. Soc., 27, 2-3, 1859-1863 (2007)
(8) D. N. Boccaccini, M. Romagnoli, P. Veronesi, M. Cannio, C. Leonelli, G. Pellacani, T. Volkov-Husovic, A. R. Boccaccini, Quality control and thermal shock damage characterization of high-temperature ceramics by ultrasonic pulse velocity testing, Int. J. Appl. Ceram. Technol., 4, 3, 260-268 (2007)
(9) M. Posarac, M. Dimitrijevic, T. Volkov-Husovic, A. Devecerski, B. Matovic, Determination of thermal shock resistance of silicon carbide/cordierite composite material using nondestructive test methods, J. Eur. Ceram. Soc., 28, 6, 1275-1278 (2008)
(10) M. Posarac, M. Dimitrijevic, T. Volkov-Husovic, J. Majstorovic, B. Matovic, The ultrasonic and image analysis method for non-destructive quantification of the thermal shock damage in refractory specimens, Materials and Design, 30, 8, 3338-3343 (2009)
(11) Y. Matsuo, T. Okajima, R. Furushima, K. Yasuda, T. Shiota, T. Ikemoto, K. Goto, T. Matsui, Damage evaluation of alumina-graphite refractories subjected to thermal shock and mechanical stress using ultra-sonic pulse-echo method, J. Tech. Assoc. Refract., 27, 2, 133 (2007)
(12) H. Carreon, A. Ruiz, A. Medina, G. Barrera, J. Zarate, Characterization of the alumina-zirconia ceramic system by ultrasonic velocity measurements, Materials Characterization, 60, 8, 875-881 (2009)
(13) M. H. Badr, L. M. Sharaf El-Deen, A. H. Khafagy, D. U. Nassar, Structural and mechanical properties characterization of barium strontium titanate (BST) ceramics, J. Electroceram., 27, 3-4, 189-196 (2011)
(14) J. Bentama, A. El Ghzizal, J. -Y. Ferrandis, Ultrasonic waves for characterisation of clay membranes, Desalination, 206, 1-3, 1-8 (2007)
(15) A. Díaz, S. Hampshire, J. -F. Yang, T. Ohji, S. Kanzaki, Comparison of mechanical properties of silicon nitrides with controlled porosities produced by different fabrication routes, J. Am. Ceram. Soc., 88, 3, 698-706 (2005)
(16) K. K. Phani, Estimation of elastic properties of porous ceramic using ultrasonic longitudinal wave velocity only, J. Am. Ceram. Soc., 90, 7, 2165-2171 (2007)
(17) K. K. Phani, A novel method of predicting ultrasonic and elastic properties of isotropic ceramic materials after sintering from the properties of partially sintered or green compacts, J. Am. Ceram. Soc., 91, 1, 215-222 (2008)
(18) A. Nishara, V. Rajendran, T. Jayakumar, P. Palanichamy, N. Priyadharsini, S. Aravindan, B. Ray, On-line ultrasonic velocity measurements for characterisation of microstructural evaluation during thermal aging of β-quenched zircaloy-2, Mater. Charact., 58, 6, 563-570 (2007)
(19) G. M. Revel, Measurement of the apparent density of green ceramic tiles by a non-contact ultrasonic method, Experimental Mechanics, 47, 5, 637-648 (2007)
(20) P. Pietroni, G. M. Revel, Laser ultrasonics for quality control in the ceramic industry, Xth World Congress on Ceramic Tile Quality, Castellón, Spain, p.bc 345-358 (2008)
(21) V. Cantavella, D. Llorens, A. Mezquita, C. Moltó, M. C. Bhardwaj, P. Vilanova, J. Ferrando, S. Maldonado-Zagal, Use of ultrasound techniques to measure green tile bulk density and optimise the pressing process, IXth World Congress on Ceramic Tile Quality, Castellon, Spain, p.bc 161-174 (2006)
(22) K. Kawasaki, NGK Insulators Ltd., Ultrasonic testing method, United States patent 5001674 (1991)
(23) Nondestructive Evaluation and Quality Control, 9th ed., ASM Handbook, Volume 17, ASM International, ASM Handbook Committee, The Materials Information Society, Metals Park, Ohio, 241-253 (1989)
(24) E. Biagi, A. Fort, L. Masotti, L. Ponziani, Ultrasonic high resolution images for defect detection in ceramic materials, Res. Nondestr. Eval., 6, 4, 219-226 (1995)
(25) M. C. Bhardwaj, I. Neeson, G. Stead, Introduction to contact-free ultrasonic characterization and analysis of consolidated materials, NDT.net, 5, 6 (2000)
(26) M. C. Bhardwaj, Non-contact ultrasonic characterization of ceramics and composites, Nondestructive Evaluation of Ceramics, C. H. Shilling, J. N. Gray (Ed.), The American Ceramic Society, Westerville, Ohio, Ceramic Transactions, 89, 265-281 (1997)
(27) M. Romagnoli, M. Burani, G. Tari, J. M. F. Ferreira, A non-destructive method to assess delamination of ceramic tiles, J. Eur. Ceram. Soc., 27, 2-3, 1631-1636 (2007)
(28) B. Hayes, Special report/R and D overview: advancing ceramic and glass technology, Ceramic Industry, 157, 8, 24-28 (2007)
(29) R. Brennan, R. Haber, D. Niesz, J. McCauley, Ultrasonic evaluation of high-density silicon carbide ceramics, Int. Appl. Ceram. Technology, 5, 2, 210-218 (2008)
(30) D. E. Johnson, J. R. Johnson, J. L. Hilburn, Electric Circuit Analysis, 2nd ed., Prentice-Hall Inc., Englewood Cliffs, New Jersey, U.S.A., 509-511 (1992)
(31) H. Abe, T. Hotta, M. Naito, N. Shinohara, K. Uematsu, Direct observation of detrimental defects in ceramics, Am. Ceram. Soc. Bull., 81, 1, 31-34 (2002)
(32) E. S. Kayalı, N. Eruslu, M. Ürgen, Y. Taptık, H. Çimenoğlu, Failure Analysis Seminar Notes, UCTEA Chamber of Metallurgical Engineers, 8-36 (1997)

Recibido: 10/11/2010
Aceptado: 20/03/2012